A massive stellar bulge in a regularly rotating galaxy 1.2 billion years after the Big Bang

Federico Lelli,[1,2,*], Enrico Di Teodoro[3], Filippo Fraternali[4], Allison W.S. Man[5], Zhi-Yu Zhang[6], Carlos De Breuck[7], Timothy A. Davis[1], Roberto Maiolino[8,9]

[1]School of Physics and Astronomy, Cardiff University,
Cardiff CF24 3AA, United Kingdom; *e-mail: LelliF@cardiff.ac.uk

[2]Arcetri Astrophysical Observatory, INAF, Florence 50125, Italy

[2]Department of Physics & Astronomy, Johns Hopkins University,
Baltimore MD 21218, United States of America

[3]Kapteyn Astronomical Institute, University of Groningen,
Groningen 9700 AV, The Netherlands

[4]Dunlap Institute for Astronomy & Astrophysics, University of Toronto,
Toronto ON M5S 3H4, Canada

[5]School of Astronomy and Space Science, Nanjing University,
Nanjing 210023, P.R. China

[6]European Southern Observatory, Germany Headquarters,
Garching bei München 85748, Germany

[7]Kavli Institute for Cosmology, University of Cambridge,
Cambridge CB3 0HA, United Kingdom

[8]Cavendish Laboratory, University of Cambridge,
Cambridge CB3 0HE, United Kingdom

Cosmological models predict that galaxies forming in the early Universe experience a chaotic phase of gas accretion, followed by gas ejection due to feedback processes. Galaxy bulges may assemble later via mergers or internal evolution. We present submillimeter observations with a spatial resolution of 700 parsecs of ALESS 073.1, a starburst galaxy at $z \simeq 5$, when the Universe was 1.2 Gyr old. Its cold gas forms a regularly rotating disk with negligible non-circular motions. The galaxy rotation curve requires the presence of a central bulge in addition to a star-forming disk. We conclude that massive bulges and regularly rotating disks can form more rapidly in the early Universe than predicted by models of galaxy formation.

In the standard Λ Cold Dark Matter (ΛCDM) cosmological model, galaxies form inside dark matter (DM) halos when primordial gas cools, collapses, and begins star formation (*1*). At early times, when the Universe was only 10% of its current age (redshift $z \simeq 5$), galaxies are predicted to undergo a turbulent phase of gas accretion from the cosmic web, leading to violent bursts of star formation and black-hole growth (*2*), rapidly followed by massive gas outflows due to feedback from supernovae and active galactic nuclei (AGN). Strong stellar and AGN feedback are needed in ΛCDM models to recover the observed number of galaxies per unit volume per unit mass (the galaxy stellar mass function) and to quench star formation in the most massive DM halos, reproducing the observed population of quiescent early-type galaxies at $z = 0$ (*3*). In the hierarchical ΛCDM scenario, the central, spheroidal-like, high-density stellar components of massive galaxies (bulges) are expected to form either after the dissipative merger of two galaxies of similar mass, or via secular dynamical processes within the stellar disk (*4*). Observing galaxies at high redshifts can test these scenarios by searching for these physical processes in action.

The 158-μm emission line of singly ionized carbon, [C II], is a major coolant of the interstel-

lar medium and traces a combination of atomic and molecular hydrogen. The [C II] line has been observed up to $z \simeq 7.5$ (*5*) and several rotating disks have been identified at $z > 3$ (*6*–*8*). Most existing observations barely resolve the [C II] distribution and kinematics, so cannot distinguish between rotating disks, galaxy mergers, or gas inflows/outflows. Limited spatial resolution has prevented the measurement of well-sampled rotation curves (with more than 5-6 independent elements), which can be used to measure different mass components using dynamical models.

We used the Atacama Large Millimeter/submillimeter Array (ALMA) to observe a star-forming galaxy at $z = 4.75$ (*6*) at a spatial resolution of about $0.11''$, corresponding to 0.7 kpc in a ΛCDM cosmology (*9*). ALESS 073.1 (LESS J033229.3-275619) was originally identified as a strong sub-millimeter source (*10*). Its large far-infrared luminosity suggests an on-going starburst with an estimated star-formation rate of about 1000 solar masses ($M_\odot$) per year (*10, 11*). ALESS 073.1 contains a dust-obscured AGN (*12*). These extreme properties indicate that the galaxy may drive a massive gas outflow (*11*). Previous [C II] observations with ALMA pointed to a rotating disk (*6*), but the low spatial resolution ($0.5''$ corresponding to $\sim$3 kpc) was insufficient to determine its detailed properties or identify gas inflows/outflows.

Figure 1-A shows the continuum map at rest-frame 160 μm, which traces dust heated by the star-formation activity. Figure 1-B shows the [C II] intensity map, which traces the cold gas distribution. The [C II] emission is about two times more extended than the dust emission and shows an asymmetry to the North-East. Similar lopsided gas disks are common in the nearby Universe, forming nearly half of the local population of atomic gas disks (*13*).

The [C II] velocity field (moment-one map; Fig. 1-C) shows a regularly rotating disk. Rotating disks and galaxy mergers may be difficult to distinguish when observed at low spatial resolutions (*14*). This is not the case for ALESS 073.1 because the area with detectable [C II] emission is covered by about 45 resolution elements. The kinematic major axis is perpendicular to the kinematic minor axis, implying that non-circular motions are negligible in the inner parts

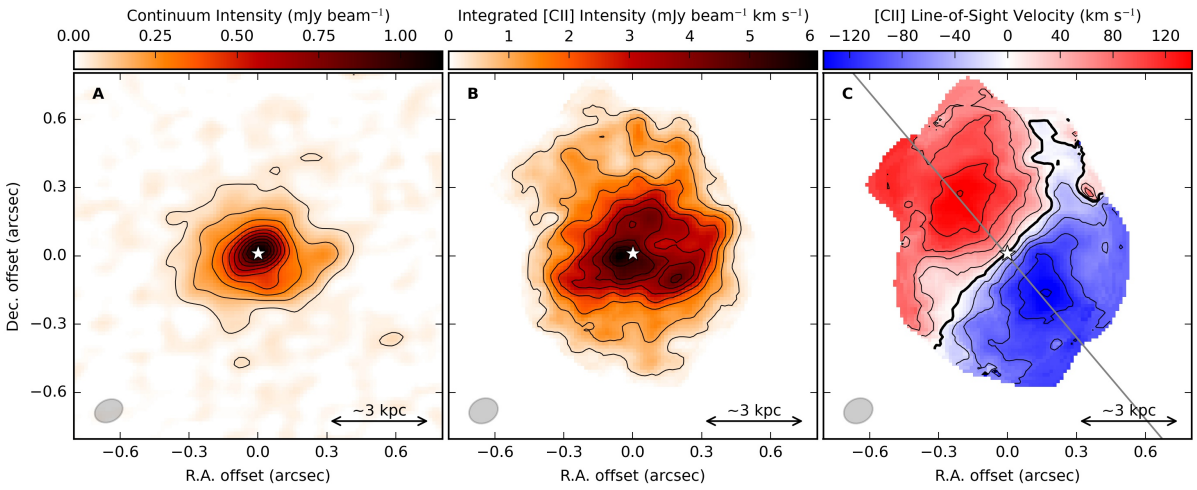

Figure 1: **ALMA observations of ALESS 073.1.** (**A**) continuum emission at 160 μm (rest-frame) tracing dust heated by young stars, (**B**) [C II] intensity map tracing cold gas, and (**C**) [C II] velocity field showing a rotating disk. North is up and East is left. The kinematic centre, located at a Right Ascension (R.A.) of $03^{\rm h}\ 32^{\rm m}\ 29.295^{\rm s}$ and Declination (Dec.) of $-27^\circ\ 56'\ 19.60''$, is shown with a white star. The beam size is plotted as the grey ellipse in the bottom-left corner. The physical scale is indicated by the scale bar in the bottom-right corner. In panel A, iso-emission contours range from 0.055 to 1 mJy beam^{-1} (where 1 mJy = 10^{-29} W m^{-2} Hz^{-1}) in steps of 0.11 mJy beam^{-1}. In panel B, iso-emission contours range from 0.35 to 6 mJy beam^{-1} km s^{-1} in steps of 0.7 mJy beam^{-1} km s^{-1}. In panels A and B, the lowest iso-emission contour corresponds to a signal-to-noise ratio of about 3. In panel C, iso-velocity contours range from -120 to $+120$ km s^{-1} in steps of 30 km s^{-1}; the bold contour indicates the systemic velocity (set to zero); the grey line shows the kinematic major axis.

of the gas disk (*15*). The gas kinematics are less regular in the North-Eastern extension: this may be due to recently accreted gas, a warped outer disk, or streaming motions along a spiral arm (*9*). The limited signal-to-noise ratio in the outer regions does not allow us to distinguish between these possibilities. Overall, the kinematic regularity of the [C II] disk is unexpected for a starburst AGN-host galaxy at $z \simeq 0$.

We model the [C II] kinematics using the software ^{3D}Barolo (*17*), which fits the observational data with a rotating disk model (*9*). This determines the [C II] surface brightness profile, the rotation curve, and the intrinsic velocity dispersion profile. The best-fitting rotation curve (Fig. 2-A) rises steeply in the central parts, declines across the disk, and possibly flattens in the outer parts, as suggested by the open velocity contours in the outer parts of the velocity field (Fig. 1-C). Similar rotation curves are observed in bulge-dominated disk galaxies in the nearby Universe (*18–20*), so there might be a bulge component in ALESS 073.1. The normalization of the rotation curve depends on the disk inclination, which we treat as a free parameter below.

We use the derived rotation curve to constrain the mass distribution within the galaxy. Our fiducial mass model has four components: cold gas disk, stellar disk, stellar bulge, and DM halo. We also investigate mass models with three components, which we find cannot plausibly fit the observations (*9*). We assume that the [C II] density profile traces the distribution of the cold gas disk, while the dust density profile traces the distribution of the stellar disk (Fig. 2-B) because dust absorbs ultraviolet radiation from young stars and re-emits it at far-infrared wavelengths. The two additional components (bulge and DM halo) are modeled with analytic functions (*9*). The bulge component implicitly includes the contribution of the central super-massive black hole, which contribute less than 10% of the central mass in high-z galaxies (*8*).

For the maximum-probability inclination of 22°, the [C II] disk rotates at velocities (V) of 300-400 km s^{-1} (Fig. 2-A). Similar rotational speeds are observed in the most massive early-type galaxies at $z = 0$ hosting molecular gas disks (*21*), so we conclude that they are the likely

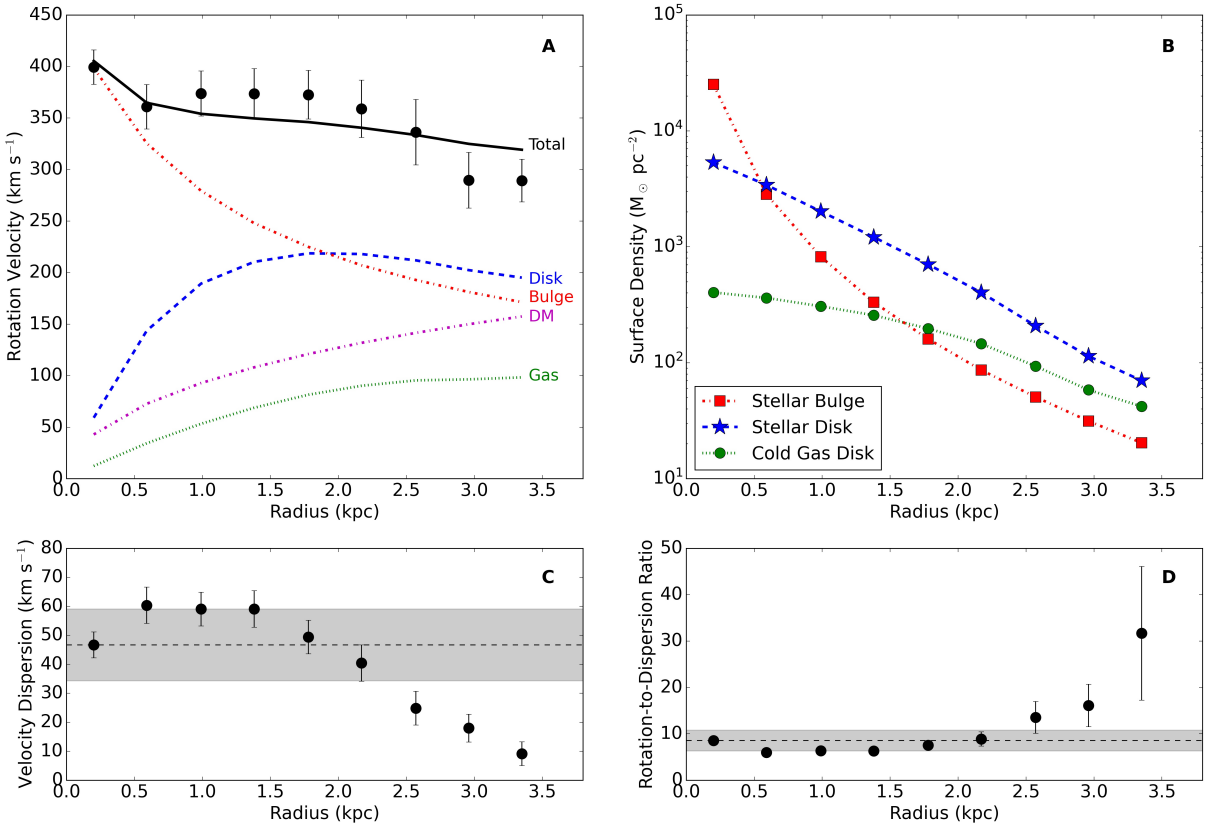

Figure 2: **Mass model of ALESS 073.1.** (**A**): the observed rotation curve (black circles with 1-sigma error bars) adopting the best-fitting inclination of 22°. The model rotation curve (solid black line) is the total of contributions from the stellar bulge (dot-dashed red line), stellar disk (dashed blue line), cold gas disk (green dotted line), and DM halo (dash-dotted magenta line). (**B**): surface density profiles of bulge (red squares), stellar disk (blue stars), and cold gas disk (green circles) adopting the best-fitting masses (*9*). The bulge profile assumes a De Vaucouleurs' surface density distribution (*16*). The stellar and gas disk profiles are obtained from azimuthal averages of the dust continuum and [C II] intensity maps, respectively. The uncertainties on these profiles are dominated by the systematic uncertainty on the normalizing masses (*9*). (**C**): the [C II] velocity dispersion profile. (**D**): disk rotational support versus radius. In panels C and D, the dashed line and grey band show the median value and median absolute deviation, respectively.

descendants of galaxies similar to ALESS 073.1. The intrinsic velocity dispersion (Fig. 2-C) reaches 50-60 km s^{-1} at small radii and decreases to 10-20 km s^{-1} in the outer parts. The ratio of rotation velocity to velocity dispersion (Fig. 2-D) is around ten within 2.5 kpc, similar to cold gas disks at $z = 0$ (*22*). The [C II] disk of ALESS 073.1 is supported by rotation, not turbulence.

The bulge component of the model is necessary to reproduce the observed high rotation speeds at small radii. We obtain a bulge-to-total mass ratio $M_{\rm bul}/M_{\rm baryon} = 0.44$, where $M_{\rm baryon}$ is given by the sum of all baryonic (non-dark matter) components within 3.5 kpc. This ratio is nearly independent of i because it is largely driven by the shapes of the observed rotation curve and of the baryonic gravitational contributions, not by their absolute normalizations. Baryons dominate the gravitational potential within 3.5 kpc, similar to massive galaxies at $z = 0$ (*20*) and $z = 1 - 3$ (*23, 24*). In a ΛCDM cosmology, DM halos are expected to have low concentrations at high z, while baryons can efficiently cool and collapse to the bottom of the potential well reaching high concentrations, so DM halos become gravitationally dominant at large radii.

Gas disks in the early Universe are expected to be more turbulent than their local analogues: the gas velocity dispersion (σ_V) is found to increase with redshift, while the degree of rotational support (V/σ_V) decreases (*22, 25*). The enhanced turbulence may be driven by gravitational instabilities from cold gas flows, and/or by stellar and AGN feedback (*26*). The low spatial resolution of the observations, however, can bias the measurements of V and σ_V (beam smearing effects), leading to systematic overestimates of σ_V and underestimates of V/σ_V (*27*).

The gas velocity dispersion of ALESS 073.1 is consistent with the extrapolations from data at $z < 3.5$. Despite hosting a starburst and a dust-obscured AGN, the galaxy lies at the low $\sigma_{\rm V}$ boundary of the values predicted by a semi-empirical model based on Toomre's disk instability parameter (Fig. 3-A), which has been invoked to describe kinematic measurements at $z < 3.5$ (*22*). The disk rotational support of ALESS 073.1 (V/σ_V-ratio) is much higher than the value predicted by the semi-empirical model (*22*), while it is similar to that of gas disks in the local

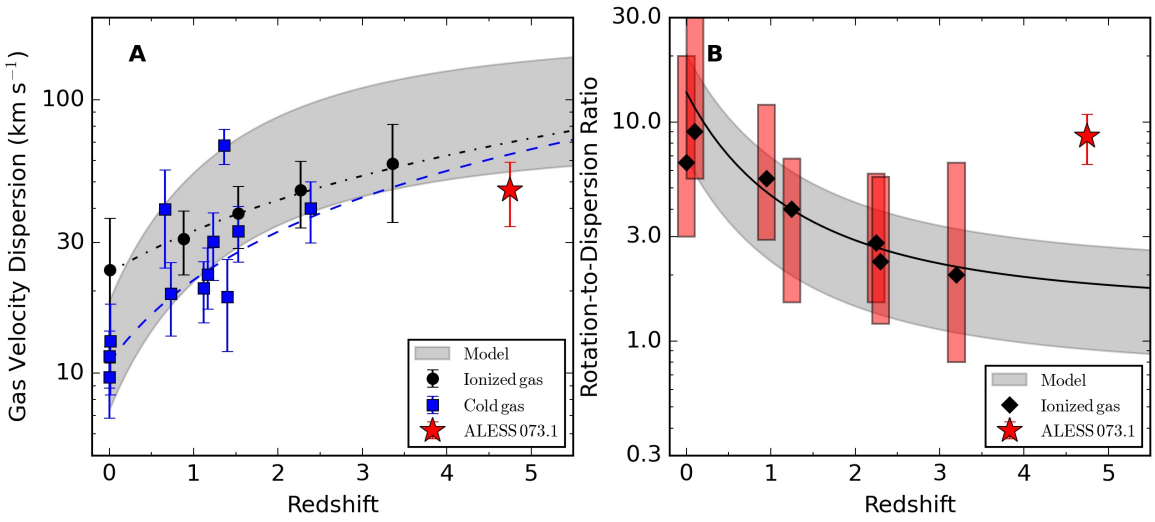

Figure 3: **Turbulence (A) and rotational support (B) of galaxies as a function of cosmic time.** Grey bands show a semi-empirical model based on Toomre's disk instability parameter (*22*). In panel A, the black, dot-dashed line and the blue, dashed line show the velocity dispersion evolution inferred from warm ionized gas data (black circles; averages from galaxy samples) and cold neutral gas data (blue squares; averages for $z = 0$ and individual galaxies for $z > 0.5$), respectively (*25*). In panel B, black diamonds and red bars show, respectively, the median and 90% distribution of ionized-gas surveys (*22*). The red star shows ALESS 073.1.

Universe (Fig. 3-B). This suggests that both starburst and AGN feedback have only a gentle effect on the cold interstellar medium of ALESS 073.1 because the [C II] disk is regular and unperturbed, contrary to galaxy formation models with violent feedback.

It remains unknown whether bulges exist in the early Universe ($z > 4$), given the lack of high-resolution infrared images probing the stellar mass distribution. In ALESS 073.1 we use the gas kinematics to infer the presence of a central massive component that is not traced by the dust. This is likely a stellar bulge hosting a super-massive black hole. Bulges form either from the secular evolution of stellar disks or after major galaxy mergers (*4*). Both mechanisms could be at play in ALESS 073.1, but they must act on short timescales because the Universe was only 1.2 Gyr old at $z \simeq 4.75$. Any major merger must have happened at even earlier cosmic epochs to provide time for the gas kinematics to relax to regular rotation. The orbital time at the last measured point of the rotation curve is 5×10^7 yr and about 5 revolutions may be required to relax the disk, so any major merger must have happened at $z > 5.5$. ALMA observations of a quasar-host galaxy at $z \simeq 6.6$ with similar spatial resolution show that the [C II] kinematics can be heavily disturbed at this younger epoch ($\sim$0.8 Gyr after the Big Bang), possibly due to mergers or interactions (*28*). Bulges may also form from star formation inside AGN-driven gas outflows (*29, 30*), which could occur on short timescales. Although we only observe a single object, we conclude that the Universe produced regularly rotating galaxy disks with prominent bulges in less than 10% of its current age. This implies that the formation of massive galaxies and their central bulges must be a fast and efficient process.

Acknowledgments

We thank Louis Legrand and Hannah Übler for providing tabular data from their publications. FL thanks Pengfei Li for technical support with the Markov-Chain-Monte-Carlo fitting code.

Funding: AWSM is supported by a Dunlap Fellowship at the Dunlap Institute for Astronomy & Astrophysics, funded through an endowment established by the David Dunlap family and the University of Toronto. RM acknowledges ERC Advanced Grant 695671 "QUENCH" and support by the Science and Technology Facilities Council (STFC).

Authors contributions: FL: conceptualization, data curation, formal analysis, investigation, methodology, project administration, validation, visualization, writing - original draft. EdT: conceptualization, formal analysis, methodology, software, visualization, writing - review & editing. FF: conceptualization, methodology, software, writing - review & editing. AWSM: formal analysis, writing - review & editing. ZYZ: formal analysis, writing - review & editing. CdB: data curation, writing - review & editing. TAD: resources, writing - review & editing. RM: resources, writing - review & editing.

Competing interests: The authors have no competing interests.

Data and materials availability: This paper makes use of the following ALMA data: ADS/JAO.ALMA#2015.1.00456.S, #2017.1.01471.S, and #2011.0.00124.S. ALMA is a partnership of ESO (representing its member states), NSF (USA) and NINS (Japan), together with NRC (Canada), MOST and ASIAA (Taiwan), and KASI (Republic of Korea), in cooperation with the Republic of Chile. The Joint ALMA Observatory is operated by ESO, AUI/NRAO and NAOJ. The raw data are available at the ALMA archive (https://almascience.eso.org/asax/). The paper also makes us of an Hubble Space Telescope image (dataset ibeuglqlq) from proposal ID 12061 available at https://archive.stsci.edu/hst/. The data cubes, moment maps, and mass models are available as supplementary data files.

Supplementary materials

Materials and Methods

Figs. S1 to S6

Table S1

References *(31-72)*

References

1. S. D. M. White, M. J. Rees, *Mon. Not. R. Astron. Soc.* **183**, 341 (1978).

2. A. Dekel, Y. Birnboim, *Mon. Not. R. Astron. Soc.* **368**, 2 (2006).

3. M. Vogelsberger, *et al.*, *Nature* **509**, 177 (2014).

4. J. Kormendy, J. Kennicutt, Robert C., *Annu. Rev. Astron. Astrophys.* **42**, 603 (2004).

5. E. Bañados, *et al.*, *Astrophys. J.* **881**, L23 (2019).

6. C. De Breuck, *et al.*, *Astron. Astrophys.* **565**, A59 (2014).

7. G. C. Jones, *et al.*, *Astrophys. J.* **850**, 180 (2017).

8. A. Pensabene, *et al.*, *Astron. Astrophys.* **637**, A84 (2020).

9. Materials and methods are available as supplementary materials.

10. K. E. K. Coppin, *et al.*, *Mon. Not. R. Astron. Soc.* **395**, 1905 (2009).

11. R. Gilli, *et al.*, *Astron. Astrophys.* **562**, A67 (2014).

12. R. Gilli, *et al.*, *Astrophys. J.* **730**, L28 (2011).

13. R. Sancisi, F. Fraternali, T. Oosterloo, T. van der Hulst, *Astron. Astrophys. Rev.* **15**, 189 (2008).

14. S. M. Sweet, *et al.*, *Mon. Not. R. Astron. Soc.* **485**, 5700 (2019).

15. F. Fraternali, T. Oosterloo, R. Sancisi, G. van Moorsel, *Astrophys. J.* **562**, L47 (2001).

16. G. de Vaucouleurs, *Annales d'Astrophysique* **11**, 247 (1948).

17. E. M. Di Teodoro, F. Fraternali, *Mon. Not. R. Astron. Soc.* **451**, 3021 (2015).

18. S. Casertano, J. H. van Gorkom, *Astron. J.* **101**, 1231 (1991).

19. E. Noordermeer, J. M. van der Hulst, R. Sancisi, R. S. Swaters, T. S. van Albada, *Mon. Not. R. Astron. Soc.* **376**, 1513 (2007).

20. F. Lelli, S. S. McGaugh, J. M. Schombert, *Astron. J.* **152**, 157 (2016).

21. T. A. Davis, *et al.*, *Mon. Not. R. Astron. Soc.* **455**, 214 (2016).

22. E. Wisnioski, *et al.*, *Astrophys. J.* **799**, 209 (2015).

23. F. Lelli, *et al.*, *Mon. Not. R. Astron. Soc.* **479**, 5440 (2018).

24. R. Genzel, *et al.*, *Nature* **543**, 397 (2017).

25. H. Übler, *et al.*, *Astrophys. J.* **880**, 48 (2019).

26. M. D. Lehnert, *et al.*, *Astrophys. J.* **699**, 1660 (2009).

27. E. M. Di Teodoro, F. Fraternali, S. H. Miller, *Astron. Astrophys.* **594**, A77 (2016).

28. B. P. Venemans, *et al.*, *Astrophys. J.* **874**, L30 (2019).

29. W. Ishibashi, A. C. Fabian, *Mon. Not. R. Astron. Soc.* **441**, 1474 (2014).

30. R. Maiolino, *et al.*, *Nature* **544**, 202 (2017).

31. B. Gullberg, *et al.*, *Astrophys. J.* **859**, 12 (2018).

32. J. P. McMullin, B. Waters, D. Schiebel, W. Young, K. Golap, *Astronomical Data Analysis Software and Systems XVI*, R. A. Shaw, F. Hill, D. J. Bell, eds. (2007), vol. 376 of *Astronomical Society of the Pacific Conference Series*, p. 127.

33. D. S. Briggs, *American Astronomical Society Meeting Abstracts* (1995), vol. 187 of *American Astronomical Society Meeting Abstracts*, p. 112.02.

34. M. G. R. Vogelaar, J. P. Terlouw, *Astronomical Data Analysis Software and Systems X*, F. R. Harnden, Jr., F. A. Primini, H. E. Payne, eds. (2001), vol. 238 of *Astronomical Society of the Pacific Conference Series*, p. 358.

35. Planck Collaboration, *et al.*, *Astron. Astrophys.* **641**, A6 (2020).

36. F. Lelli, M. Verheijen, F. Fraternali, *Mon. Not. R. Astron. Soc.* **445**, 1694 (2014).

37. F. Lelli, M. Verheijen, F. Fraternali, R. Sancisi, *Astron. Astrophys.* **537**, A72 (2012).

38. F. Lelli, M. Verheijen, F. Fraternali, R. Sancisi, *Astron. Astrophys.* **544**, A145 (2012).

39. T. A. Davis, M. Bureau, M. Cappellari, M. Sarzi, L. Blitz, *Nature* **494**, 328 (2013).

40. C. Trachternach, W. J. G. de Blok, F. Walter, E. Brinks, J. Kennicutt, R. C., *Astron. J.* **136**, 2720 (2008).

41. C. Y. Peng, L. C. Ho, C. D. Impey, H.-W. Rix, *Astron. J.* **139**, 2097 (2010).

42. J. A. Hodge, *et al.*, *Astrophys. J.* **876**, 130 (2019).

43. E. Athanassoula, *Astron. Astrophys.* **69**, 395 (1978).

44. M. Thomasson, *et al.*, *A&A* **211**, 25 (1989).

45. S. Casertano, *Mon. Not. R. Astron. Soc.* **203**, 735 (1983).

46. J. A. Sellwood, *Galaxy Dynamics - A Rutgers Symposium*, D. R. Merritt, M. Valluri, J. A. Sellwood, eds. (1999), vol. 182 of *Astronomical Society of the Pacific Conference Series*, p. 351.

47. P. C. van der Kruit, K. C. Freeman, *Annu. Rev. Astron. Astrophys.* **49**, 301 (2011).

48. E. Noordermeer, *Mon. Not. R. Astron. Soc.* **385**, 1359 (2008).

49. C. Gall, J. Hjorth, A. C. Andersen, *Astron. Astrophys. Rev.* **19**, 43 (2011).

50. G. Pezzulli, F. Fraternali, S. Boissier, J. C. Muñoz-Mateos, *Mon. Not. R. Astron. Soc.* **451**, 2324 (2015).

51. S. M. Kent, *Astron. J.* **91**, 1301 (1986).

52. N. A. Grogin, *et al.*, *Astrophys. J. Suppl. Ser.* **197**, 35 (2011).

53. J. A. Hodge, *et al.*, *Astrophys. J.* **833**, 103 (2016).

54. P. Lang, *et al.*, *Astrophys. J.* **879**, 54 (2019).

55. J. F. Navarro, C. S. Frenk, S. D. M. White, *Astrophys. J.* **462**, 563 (1996).

56. H. Tak, S. K. Ghosh, J. A. Ellis, *Mon. Not. R. Astron. Soc.* **481**, 277 (2018).

57. K. E. K. Coppin, *et al.*, *Mon. Not. R. Astron. Soc.* **407**, L103 (2010).

58. L. J. Tacconi, *et al.*, *Astrophys. J.* **680**, 246 (2008).

59. C. De Breuck, *et al.*, *Astron. Astrophys.* **530**, L8 (2011).

60. D. P. Stark, A. J. Bunker, R. S. Ellis, L. P. Eyles, M. Lacy, *Astrophys. J.* **659**, 84 (2007).

61. J. L. Wardlow, *et al.*, *Mon. Not. R. Astron. Soc.* **415**, 1479 (2011).

62. J. M. Simpson, *et al.*, *Astrophys. J.* **788**, 125 (2014).

63. T. Wiklind, *et al.*, *Astrophys. J.* **785**, 111 (2014).

64. J. Kormendy, L. C. Ho, *Annu. Rev. Astron. Astrophys.* **51**, 511 (2013).

65. A. Vale, J. P. Ostriker, *Mon. Not. R. Astron. Soc.* **353**, 189 (2004).

66. Q. Guo, S. White, C. Li, M. Boylan-Kolchin, *Mon. Not. R. Astron. Soc.* **404**, 1111 (2010).

67. L. Legrand, *et al.*, *Mon. Not. R. Astron. Soc.* **486**, 5468 (2019).

68. A. A. Dutton, A. V. Macciò, *Mon. Not. R. Astron. Soc.* **441**, 3359 (2014).

69. D. Foreman-Mackey, D. W. Hogg, D. Lang, J. Goodman, *PASP* **125**, 306 (2013).

70. D. Foreman-Mackey, *The Journal of Open Source Software* **1**, 24 (2016).

71. M. Milgrom, *Astrophys. J.* **270**, 365 (1983).

72. C. Skordis, T. Złosnik, *arXiv e-prints* p. arXiv:2007.00082 (2020).